UV-assisted reduction of graphite oxide to graphene by using a photoinitiator

Bing Xue[1], Yingquan Zou[1,*] , and Yuchun Yang[2]

[1] *College of Chemistry, Beijing Normal University, Beijing 100875, China*
[2] *Shenzhen Rongda Photosensitive Science and Technology Co., Ltd, Shenzhen 518103, China*

ABSTRACT

Being a highly promising material, graphene has triggered a great attention within researchers as-well-as has obtained some achievements in specific application areas. However, applying graphene to electronic devices via a facile method has proven to be difficult. Here, we have fabricated graphene by reducing graphene oxide (GO) under a 395 nm ultraviolet (UV) irradiation in a suspension containing Bis(cyclopentadienyl)bis[2,6-difluoro-3-(1-pyrryl)phenyl]titanium (GR-FMT) and GO. GR-FMT is an efficient free-radical type of photoinitiator, which is commonly used in photoresists. GO quickly reduces to graphene by accepting electrons generated by the decomposition of the GR-FMT photoinitiator under UV irradiation. Here, the GR-FMT plays both reductant and deoxidant roles and highly improves the reducing reaction efficiency. Photo etching is a commonly used technique in electronic device technology; however, its application to the mass production of GO, to be used in practical nano-devices and integrated circuits, is still an unresolved problem. To address this problem, in this work, graphene oxide is suspended in ethanol and it undergoes reduction by the UV-irradiated GR-FMT suspension; the corresponding mechanism is explored. This methodology turns out to be a novel and facile UV-assisted reduction technique with the advantage of being time-efficient and energy-efficient, simple, scalable, and environmental friendly.

Introduction

In recent years, a significant interest has been devoted to the development of carbon-based materials and especially graphene. Graphene is within the most promising material for electronic devices applications due to its unique electronic structure combined with outstanding thermal conductivity, large theoretical surface area, high carrier mobility, and superior intrinsic mechanics. These features make it an appealing candidate for next generation electronics, in particular for supercapacitors [1, 2], flexible electrodes [3, 4], catalyst supports [5, 6], fuel cell [7], and field-effect transistors [8]. Up to now, graphene has been designed and fabricated by many techniques

Springer

such as chemical vapor deposition (CVD) [9, 10], micromechanical exfoliation of graphite [11, 12], by unzipping carbon nanotubes [13, 14], epitaxial growth [15], and by reducing graphene oxide [16, 17]. Among them, most efforts have been directed to exfoliation and to the synthesis of graphene oxide by following ultrasonic dispersions procedures, followed by reduction through chemical method because other methods could not meet the stringent demands of large-scale production. Even though reduced graphene oxide (RGO) exhibits a considerable amount of sheet defects and a lower conductivity compared to graphene, the reduction of GO is still the most extensively used method allowing for large-scale production of graphene materials, being an effective, reliable, and low-cost method [18, 19]. To date, various reduction methods have been applied, such as, reduction by different reducing agents [20–25], thermal reduction [26], microwave reduction [27], electrochemical reduction [28], laser irradiation [29–31], and UV-assistant reduction [32, 33]. Since chemical reduction requires the extensive use of toxic chemical agents, laser reduction requires high energy, and thermal reduction requires high-temperatures, photochemical reduction is considered as one of the mildest, simplest, and most environmental friendly techniques. Moreover it can be performed without using polluting agents and can be carried out at room temperature. Nevertheless, the modification of the preparation method to get high-quality

products is still a critical step to bridge the gap between laboratory trials and the practical production of functional devices. Here, we designed a novel and facile approach for the reduction of GO by using a photoinitiator as reductant and ethanol as solvent under UV-light irradiation.

GR-FMT, a titanocene photoinitiator, can break into several intermediate radicals under UV irradiation [34]. Intermediate radicals can either recombine to form a new photoproduct or initiate the polymerization of monomers [35]. Researchers have found that some metal nanoparticles (copper, silver, and gold) can be obtained by exploiting free radicals produced by the photoinitiator under UV irradiation [36]. GO can easily disperse in many solvents due to the presence of carboxyl, carbonyl, hydroxyl, and epoxy functional groups. This makes the photo-induced chemical reduction of GO with GR-FMT feasible. Interestingly, the new design route is revealed to be time and energy-efficient, simple, environmental-friendly. Especially, it does not require the deoxidizing process, which is an advantage in respect to other photocatalytic methods for GO reduction employing TiO_2. The synthetic route is shown in Scheme 1. In order to visually enhance the results, we summarized the different GO reduction approaches to produce graphene sheets in Table 1. Compared to the results of the reported works, this work displays a shorter reaction time, a simpler process, and an easier scalability allowing for opening the way to mass
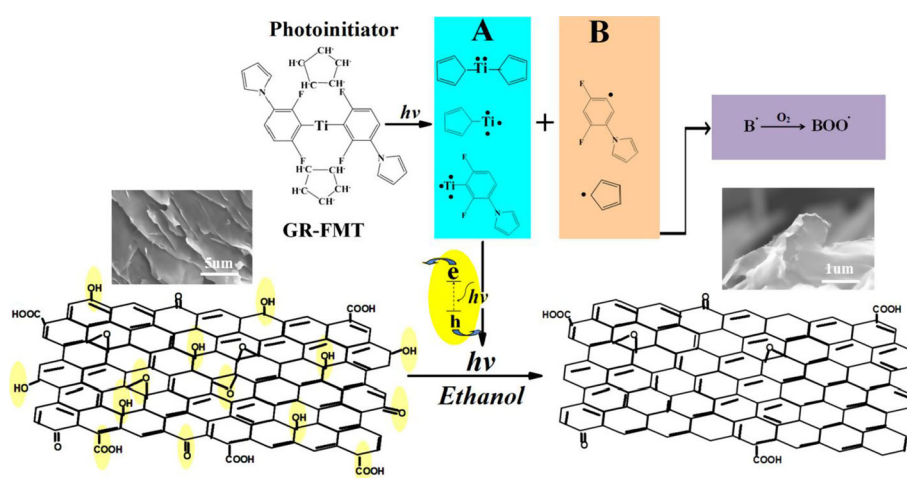
Scheme 1 How the GR-FMT photoinitiator produces free radicals when irradiated by a 395 nm UV light. Charge separation occurs in the presence of ethanol, and electrons accumulate within Ti-containing particles. Ti_{iso}^{n+}-containing particles (A-type) possess the ability to interact with GO sheets and reduce some functional groups, while particles without Ti_{iso}^{n+} (B-type) cannot accumulate electrons, so they dissolve in the solvent or combine with O_2 within the solvent, providing more opportunities for A-type particles to reduce the oxygen-containing functional groups on the GO surface.

Table 1 Comparison of a set of reduction approaches to produce graphene sheets

Methods	Solvent	Reductants	Scalability	Quality	Complexity	Period	Refs.
CR	Methanol	NaBH$_4$	High	Low	Complex	>2 h	[18]
CR	Water	Vitamin C	High	Low	Complex	24 h	[19]
CR	Ethanol/water	TiO$_2$	High	Low	Complex	1 h	[20]
CR	Serum/lactate	Bacteria/Shewanella	Low	Low	Complex	>24 h	[21]
CR	Water/NaOH	Protein/herceptin	Low	Low	Complex	–	[22]
CR	Water	hydroxylamine	High	Low	Complex	–	[23]
CR	THF	LiAlH$_4$	High	Low	Complex	>24 h	[24]
CR	Water	N$_2$H$_4$·H$_2$O	High	Low	Complex	24 h	[25]
CR	Water/ethanol	hydroquinone	High	Low	Complex	20 h	[57]
LR/532/355 nm	Water	–	Low	Low	Simple	5 min	[58]
TR	–	–	High	High	Simple	35 min	[26]
LR/788 nm	–	–	Low	High	Simple	s	[29]
LR/1064 nm	–	–	Low	High	Simple	mm s^{-1}	[30]
LR/663 nm	–	–	Low	High	Simple	15 µm s^{-1}	[59]
EUV/46.9 nm	–	–	Low	High	Simple	ns	[60]
MR	Water	–	High	Low	Simple	10 min	[27]
ECR	Water	–	Low	Low	Simple		[28]
UVR	Ethanol	TiO$_2$	High	Low	Complex	2 h	[32, 33]
UVR	Ethanol	GR-FMT	High	Low	Simple	10 min	Our work

CR chemical reduction, *LR* laser reduction, *TR* thermal reduction, *MR* microwave reduction, *ECR* electrochemical reduction, *EUV* extreme UV, *UVR* UV-assisted reduction, *THF* tetrahydrofuran

production of RGO to be used in practical nano-devices and integrated circuits.

Experimental

Graphite oxide was prepared by using graphite powder and the popular modified Hummer's method [37]. The ethanol solution was prepared by mixing GO (4 mg), the GR-FMT photoinitiator (40, 80 and 120 mg), and ethanol (20 mL) into a transparent test tube. The suspensions were irradiated by the 395 nm UV-light source placed at 15 cm distance, for 10 min at ambient temperature, and in a dark environment. The final UV-RGO films were characterized after the black precipitant was centrifuged, washed with ethanol for three times, and dried at 65 °C for 5 h. In this experiment, a 395 nm LED UV-light source (Lantian UV Co. Ltd., Zhuozhou, China) was selected. The radiation intensity was 100 mW/cm^2. The radiation intensity was measured with an actinometer built by the Photoelectric Instrument Factory of Beijing Normal University.

Structural analysis was performed on a Shimadzu model XRD-6000 X-ray powder diffractometer (Cu Kα radiation, 1.5406 Å). The quality and structure of GO and UV-RGO layers were further characterized by Fourier transform infrared spectroscopy (FTIR, IRAffinity-1/Shimadzu) in the 400–4000 cm^{-1} range, in transmission mode, by X-ray Photoelectron spectroscopy (XPS, ESCSLAB 250Xi/Thermo Fisher) and by Raman spectroscopy (LabRAM ARAMIS/Horiba Jobin–Yvon). The UV–Vis spectra were acquired on a PerkinElmer-LS55 instrument in the 200–700 nm range. TEM images and electron diffraction patterns were conducted on a TF 20 microscope (FEI). TEM samples were prepared by dropping 10 µL of supernatant, previously sonicated for 10 min, onto a holey carbon grid. The morphology of GO and UV-RGO films was characterized by scanning electron microscopy (SEM, S-4800/Hitachi) without any sample pre-treatment. The thickness of UV-RGO was measured by atomic force microscopy (AFM) (Nanoscope VIII MultiMode, Bruker) in tapping mode, with samples obtained by spin-coating alcohol suspensions onto cleaned mica wafers. Cyclic voltammetry (CV) and electrochemical impedance

spectroscopy (EIS) were performed to characterize the electrochemical properties before and after UV irradiation with a Shanghai Chenhua CHI660D electrochemical workstation. A three-electrode system was employed using a modified UV-RGO electrode as the working electrode, a platinum wire as the counter electrode, and Ag/AgCl as the reference electrode in a electrolyte solution containing 100 mM KCl and 10 mM $[Fe(CN)_6]^{4-/3-}$. EIS was performed with the same three-electrode system, at a frequency ranging from 0.1 Hz to 100 kHz. CV was recorded in the potential range from -1.0 V to 1.0 V with a potential sweep rate of 50 mVs^{-1}.

Results and discussion

XRD, FTIRF, Raman, and XPS analysis of GO and UV-RGO

It is well-known that free-radical photoinitiators have the ability to reduce metal ions [38, 39]. In this work, we used a photoinitiator to reduce GO. For this purpose, we screened three commonly used free-radical photoinitiators (GR-FMT, GR-819, and GR-TPO) and compared their reducing ability.

Absorption spectra from the three photoinitiators indicate a common absorption at 395 nm wavelength (supporting Information, Fig. S1a). Furthermore, XRD patterns of the products obtained with these three photoinitiators dispersed in methanol, ethanol, and acetone solvents have been analyzed (supporting Information, Fig. S1b). XRD spectra show that only GR-FMT presents the broad peak corresponding to RGO; the highest RGO peak belongs to products of dispersing GR-FMT in ethanol. In addition, the picture of GO/ethanol suspensions (4 mg, 20 mL) with different amounts of GR-FMT (0, 40, 80, 120 mg) after 10 min of irradiation is displayed in supporting Information, Fig. S2. Sample A refers to the solution of GR-FMT in ethanol after irradiation (no GO); sample B shows the 40 mg GR-FMT suspension exhibiting a black precipitation and a supernatant liquid is not as transparent as the one in sample D (corresponding to the 80 mg GR-FMT suspension). This is probably due to the insufficient amount of GR-FMT, which makes the supernatant liquid to contain some unreacted GO. In contrast, a yellow precipitant appears for the 120 mg GR-FMT suspension. The origin and nature of this yellow precipitation was investigated by XRD by comparing patterns from the dried yellow precipitate with the pristine GR-FMT

Fig. 1 Multiple characterizations of GO and UV-RGO. a FT-IR spectra. b Raman spectra. c XPS survey spectra. The insets show C1s spectra of GO and UV-RGO and the Ti2p spectrum. d XRD patterns of graphite, GO, and UV-RGO.
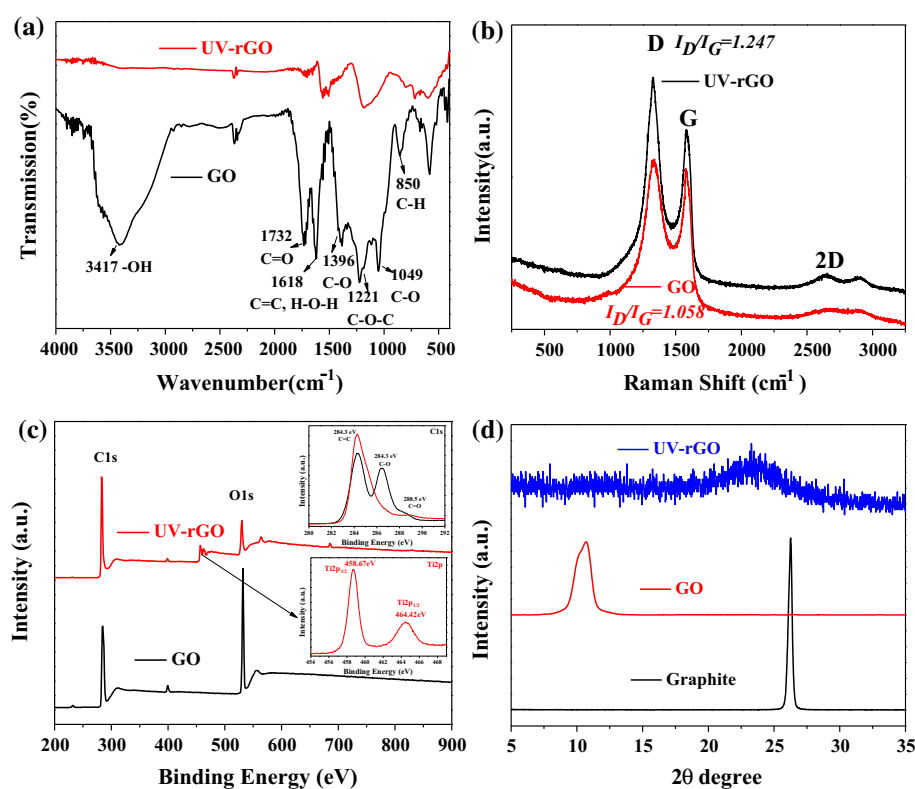
powder (supporting Information, Fig. S3). Identical patterns obviously indicate that the yellow precipitate corresponds to GR-FMT. Only sample D displays a transparent supernatant liquid and pure black precipitation. Based on the above analysis, the 80 mg suspension was finally chosen as it provides the optimum amount of GR-FMT. Further experiments and characterizations have been made on this suspension to investigate the ability of reducing GO.

FTIR spectra of GO and UV-RGO are shown in Fig. 1a. Peaks are identified as O–H stretching vibration mode ($3417 \ cm^{-1}$), C=O stretching ($1732 \ cm^{-1}$), skeletal vibrations from unoxidized graphitic domains ($1618 \ cm^{-1}$), C–O–C stretching ($1221 \ cm^{-1}$), and C–O–oxygen-containing groups vibrations (1396 and $1049 \ cm^{-1}$) [24]. In the FTIR spectrum from UV-RGO, the characteristic stretching vibrations observed in GO are almost absent due to the deoxygenating process. Although some oxygen-containing groups could still be detected in the FTIR analysis, the UV-RGO includes a small quantity of oxygen-containing functional groups indicating a successful synthesis of reduced GO by such a UV-assisted method.

To verify this result, Raman spectra were acquired with an exciting wavelength of 633 nm (Fig. 1b). Raman spectroscopy is a non-destructive technique which allows characterizing structural changes or material defects; it can thus easily provide information about the quality of the sample [40]. In graphene, the G band (at $1590 \ cm^{-1}$) is commonly attributed to the first-order scattering of E_{2g} phonons of sp^2 carbon atoms while the D band (at $1350 \ cm^{-1}$) indicates the presence of disorder and structural defects on the carbon network [41]. In Fig. 1b, the bottom solid red line shows that GO contains typical D, G, and amorphous 2D bands. The UV-RGO (solid black line) spectrum exhibits an increased D band due to an increase in edge planes and edge defects after UV irradiation [42]. The D band from both spectra indicates that sp^3 centers still exist after the reduction. The intensity ratio between D and G bands (I_D/I_G) provides further information on the defects extent on these materials. The starting intensity ratio I_D/I_G for GO is 1.058. After the UV-reduction process, the ratio increases up to 1.247, indicating a higher concentration of localized sp^3 defects and disorder with respect to the sp^2 carbon network from GO before reduction [43]. The higher I_D/I_G also testifies the existence of multiple RGO layers due to restacking [15].

To further investigate the properties and the chemical state of elements in UV-RGO material, the C:O ratio and information related to functional groups of the reduced GO have been investigated by X-ray photoelectron spectroscopy (XPS). XPS is a very sensitive analysis method which can provide the surface elemental compositions of materials [18]. Survey scans were conducted to provide the atomic composition as shown in Fig. 1c. A higher amount of oxygen-containing groups implies a lower C:O ratio. After the UV irradiation process, a higher C:O ratio is obtained demonstrating that GR-FMT reduces the GO and results in a lower amount of oxygen-containing groups. In addition, high-resolution XPS core level analysis has also been performed on C1s spectrum (see C1s inset of Fig. 1c). Two XPS components in GO sample indicate the existence of oxygen-containing functional groups. In the GO C1s spectrum, three peaks have been identified corresponding to C=C (284.3 eV), C–O (286.5 eV), and C=O (288.5 eV). Interestingly, the C=O component nearly disappears and the C–O intensity largely weakens after the UV treatment, in agreement with the smaller portion of residual oxygen-containing carbon in UV-RGO [43]. The C1s XPS spectra in Fig. 1c confirm the partial restoration of the π-electron network in UV-RGO after reduction [44]. The same conclusion was drawn by FT-IR measurement [45]. Moreover, the XPS chemical analysis of Ti2p high-resolution spectrum indicates the presence of Ti^{4+} ($Ti2p_{3/2}$ at 458.67 eV and $Ti2p_{1/2}$ at 464.42 eV), which confirms the presence of TiO_2 [46] (see the Ti2p inset of Fig. 1c).

XRD patterns of graphite, GO, and UV-RGO are shown in Fig. 1d. The interlayer distance was calculated based on the Bragg equation, $2d\sin\theta = n\lambda$, where λ is the X-ray wavelength; θ is the diffraction angle; and d is the lattice spacing. For natural graphite, the sharp reflection at 26.36° ($d = 0.338$) corresponds to the characteristic (002) diffraction. The (002) reflection shifts to 11.24° ($d = 0.787$) for GO, which is ascribed to the larger interlayer distance, indicating that GO has been completely exfoliated [44]. The broadening and shifting of the characteristic diffraction peak of graphite from 26.36° to 23.58° ($d = 0.377$) after the UV-assisted reduction can be attributed to the shorter range order within the stacks and confirms a random packing of graphene sheets in RGO [45]. This high degree of shifting also indicates that oxygen-containing functional groups are removed and thus confirms that this photochemical

process has the ability to reduce GO. To confirm that free radicals from GR-FMT can recombine after UV irradiation, we explored the GO-ethanol suspension with GR-FMT in excess, which was investigated by XRD (Supporting Information, Fig. S3). The yellow powder precipitate analysis shows no obvious difference in peaks position although the intensities are lower. This indicates that the product is not modified and that the photoinitiator GR-FMT is stable in ethanol.

UV–Vis spectra

UV–vis analysis is used to investigate the photoreaction process. In order to further confirm the reduction process and to further clarify the reaction mechanism, the photoreduction of the GO-ethanol solution under UV irradiation have been investigated by UV–vis spectroscopy. The results show no visible changes in the UV–vis spectra and that thus GO alone cannot be photoreduced when dispersed in the ethanol (Fig. 2a inset). On the other hand, the irradiation of the suspension containing the GR-FMT photoinitiator turns it immediately into a black precipitate (Fig. 2a). An ethanol suspension of GO GR-FMT kept in a dark environment for 15 days without irradiation have also been investigated (Fig. 2 (b)) showing that the UV–vis spectra and color of the suspension are almost unchanged with respect to the starting suspension. This indicates that ethanol suspensions are stable and can be stored in dark for a long period without undergoing any change. Therefore, the combination of GO, GR-FMT, and UV light is essential for the photoreduction process.

Figure 3a shows a broad absorption around 395 nm for GR-FMT in ethanol. Figure 3b shows the decrease of the absorption with the irradiation time, indicating that GR-FMT decomposes in ethanol under UV irradiation (Scheme 1). As Sabol et al. described [47], two intermediate products, photocleaved isomer (K) and an isomer (K*) are produced upon UV illumination. "K" is an unstable titanocene intermediate, and "K*" is a reversible intermediate that can return to the original form (GR-FMT). This phenomenon establishes the mediating role of Ti_{iso}^{n+}, which is similar to the one in UV-assisted GO-TiO$_2$ reduction process where Ti^{4+} centers play the role of trapping sites for photogenerated electrons [32, 48]. In this work, the UV-assisted reduction can proceed fluently without bubbling nitrogen through the
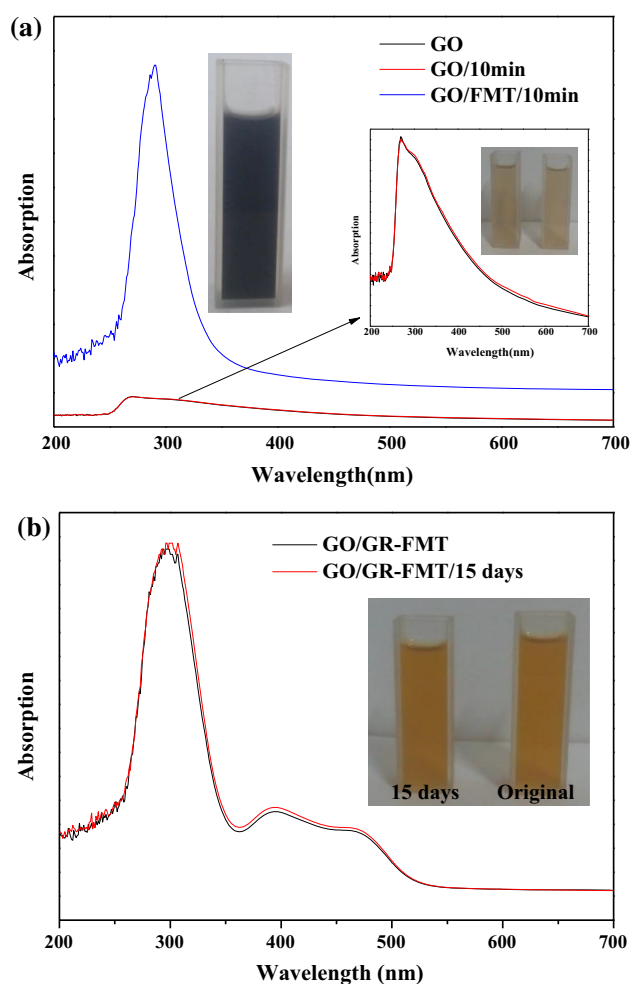

Figure 2 **a** The *inset* shows UV–Vis spectra from the irradiated (10 min) and the non-irradiated GO/ethanol solution without the photoinitiator. The high intensity line belongs to the UV–Vis spectrum of the GR-FMT photoinitiator which was added into the system before irradiation. **b** UV–Vis spectra from the GO/ethanol/GR-FMT solution stored in dark for 15 days. The *inset* shows the solution color before and after 15 days.

solution; this indicates that the amount of electrons is large enough to overcome the effect of oxygen inhibition and can thus trigger the GO reduction. Oxygen inhibition is a well-known inevitable phenomenon in the polymerization process under ambient environment operation. Ground states are generally singlet states, while O$_2$ is triplet state containing two unpaired electrons with the same spin direction, the polymerization reaction is mediated by free radicals thus resulting in their progressive consumption. In the work of Ligon et al. [49], methods for avoiding oxygen inhibition have been proposed; this includes (i) performing the reaction quickly, which prevents
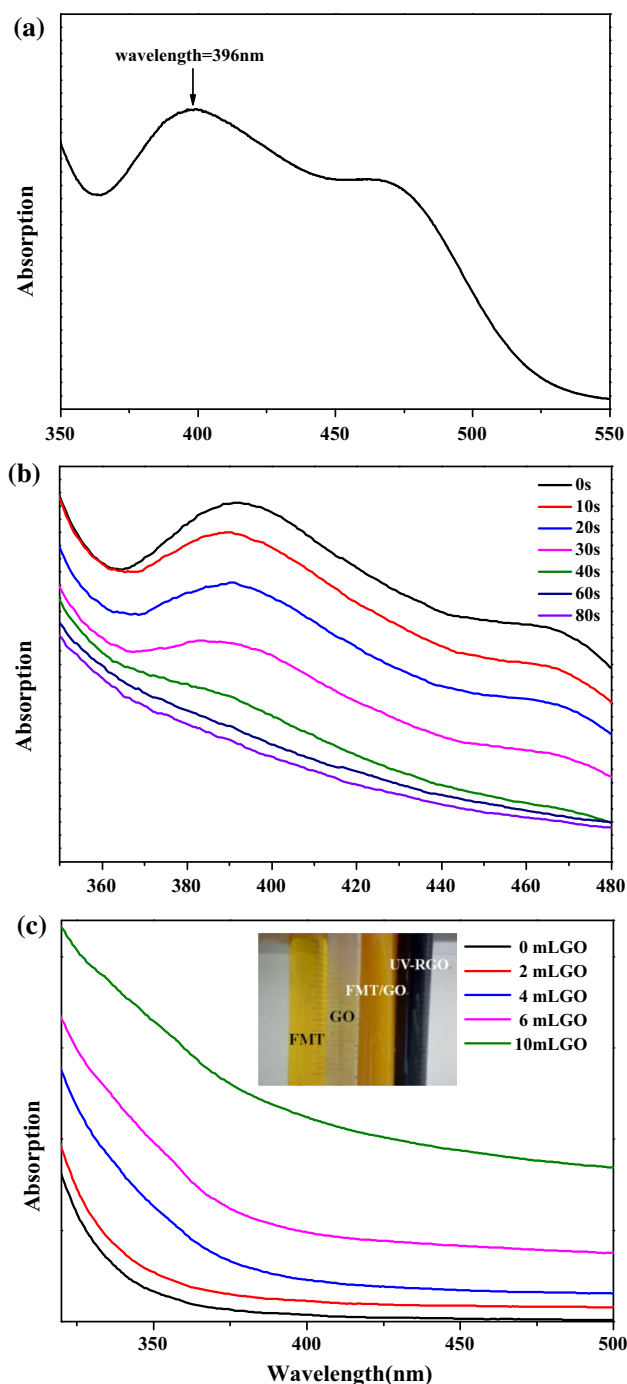
Figure 3 **a** Absorption spectra of GR-FMT dissolved in ethanol. **b** Absorption spectra of GO-GR-FMT dispersed in ethanol after 0, 10, 20, 30, 40, 60, and 80 s of UV irradiation. **c** Absorption spectra of a 20 mL ethanol solution with 80 mg of GR-FMT and different GO amounts (0, 2, 4, 6, 10 mL solution of 0.2 mg/mL concentration). The *inset* shows the color of GR-FMT, GO, GR-FMT/GO, and UV-RGO solutions.

the diffusion of O_2 from outside into the reaction system, or (ii) introducing a higher concentration of photoinitiator so that more free radicals are produced and could consume O_2. In this experiment, as illustrated in Scheme 1, free radicals produced after irradiation can be divided into two types, Ti_{iso}^{n+} containing (A) and Ti_{iso}^{n+} free (B). In the presence of ethanol, a charge separation occurs and electrons accumulate within Ti-containing particles [32]. Thus, Ti_{iso}^{n+} containing A-particles possess the ability to interact with GO sheets and to reduce certain functional groups, while B-particles, without Ti_{iso}^{n+}, cannot accumulate electrons, thus dissolve or combine with oxygen within the solvent thus favoring A-particles to reduce oxygen-containing functional groups on the GO surface.

Figure 3c displays the absorption spectra of GO and GR-FMT suspensions in ethanol with different GO contents (0, 2, 4, 6, 10 mL, of a 0.2 mg/mL solution) after UV irradiation for 10 min. The inset shows changes in color of solution of GR-FMT, GO, GR-FMT/GO, and UV-RGO. The turn from a yellow to a black color testifies the reduction of GO, which might be associated with the partial restoration of the π network within the carbon structure [50]. With a higher quantity of GO, more electrons are produced at the GR-FMT surface and transferred to GO platelets to trigger reduction. The established reaction formula is as follows:

$$GR - FMT(e^-) + GO \rightarrow GR - FMT + RGO \qquad (1)$$

Such photo-assisted GO reduction has the advantages of being environment-friendly and possibly modulated on demand by tuning the UV irradiation.

SEM, TEM, and AFM images

A considerable production of graphene was achieved by reducing a 500 mL GO/ethanol suspension (0.2 mg/mL). The morphology of GO and UV-RGO was analyzed by SEM, TEM, and AFM measurements. Figure 4a is the sketch of the UV-irradiation process. Figure 4b illustrates the experimental setup with the LED light used (inset). Figure 4c and e are the SEM micrographs of GO and UV-RGO. The RGO presents the more graphene edges. This result well agrees with the Raman analysis showing that the D

Figure 4 **a** Sketch of the UV-irradiation process. **b** Experimental setup; the *inset* shows the two possible lines of LED light. **c** and **e** SEM micrographs of GO and UV-RGO. **d** and **f** Magnified images of GO and UV-RGO under the same resolution. **g** and **h** TEM images of the GO and UV-RGO. **i** High-resolution TEM image of UV-RGO sheets. The *inset* is a typical SAED of the UV-RGO.
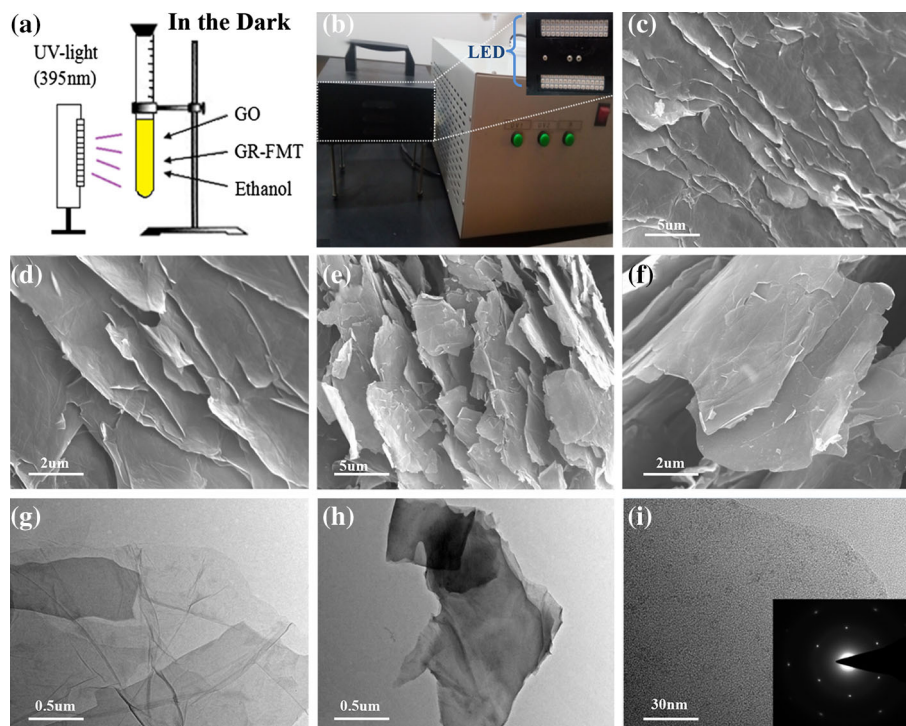
band was enhanced by the UV irradiation suggesting an increase in edge planes and edge defects. Figure 4d and f are magnified images of GO and UV-RGO. Moreover, Fig. 4g and h exhibit TEM images of GO and UV-RGO. Comparatively, the surface of GO (Fig. 4g) is smoother and presents transparent and clean lamellae forms: some wrinkles at the edges of the lamellar structure indicate the presence of fewer layers of graphene. For UV-RGO, these layers (Fig. 4h) overlap with the area of low contrast and the translucent structure, indicating the presence of a multi-layered stacked graphene. This is due to the lower quality of oxygen-containing functional groups after the reduction, thus resulting in the aggregation between the layers due to Van der Waals' interactions. The selected area electron diffraction (SAED) pattern (inset of Fig. 4i) indicates a hexagonal honeycomb structure of graphene.

Figure 5a shows a photograph of the 500 mL (0.2 mg/mL) UV-RGO suspension. Figure 5b is a picture of the UV-RGO powder. The thickness of UV-RGO sheets was measured by AFM: images and height profiles of UV-RGO are shown in Fig. 5c. Samples are prepared by drop-casting a dilute GO and UV-RGO dispersion onto a mica substrate. We can obviously observe that individual sheet height of UV-RGO is about 3.40 nm. We estimate the graphene

sheets to be tri-layer. That is ascribed to the presence of residual groups above and below the original graphene plane on UV-RGO. The irregular thickness of UV-RGO sheets testifies that defects are formed inside layer planes [51]. In addition, the AFM image of UV-RGO indicates that the height of TiO_2 nanoparticles is about 3 nm which is consistence with the work in Ref. [32].

EIS and CV analysis

The electrochemical behavior related to the electron transfer of UV-RGO and GO electrodes using an $[Fe(CN_6)]^{3-/4-}$ couple as a redox probe has been explored (Fig. 6). Electrochemical impedance spectroscopy (EIS) techniques were conducted in an electrolyte solution containing 10 mM $K_3[Fe(CN_6)]$/$K_4[Fe(CN_6)]$ and 0.1 M KCl at a scan rate of 50 mV/s. Information on the electrode surface is deduced from changes in the impedance value. The EIS analysis is completed by fitting of Nyquist plots based on the Randles equivalent circuit (Fig. 6a); this includes a half semicircle at high frequencies and a straight line at low frequencies due to electron transfer and diffusion processes, respectively. The EIS measures the resistance which includes three parts: the resistance of the electrolyte, the intrinsic resistance of the

Figure 5 a Large volume of UV-RGO suspension and a 20 mL transparent test tube. **b** UV-RGO powders obtained after solvent evaporation and drying. **c** AFM images and line profiles from UV-RGO deposited on mica substrate.
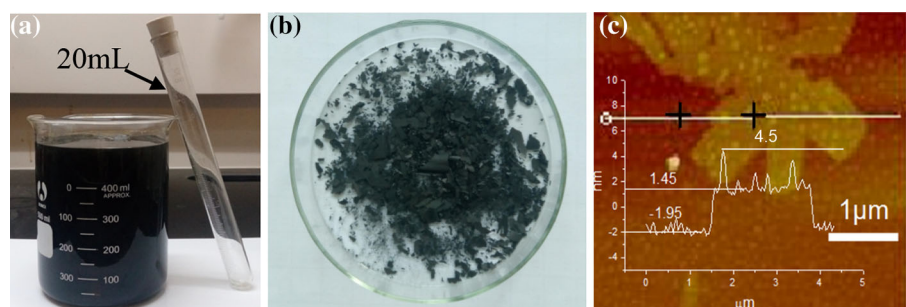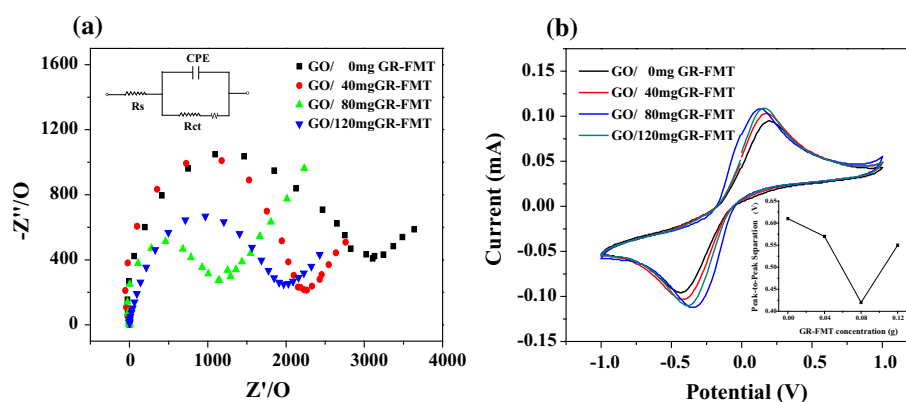

Figure 6 a Electrochemical impedance spectroscopy (EIS) measurements on UV-RGO containing different amounts of GR-FMT (0, 40, 80, and 120 mg) in 0.1 M KCl electrolyte solution containing 0.01 M Fe$(CN)_6^{3-/4-}$ obtained with scan rate of 50 mVs^{-1}. **b** CV curves of the four electrodes.

material, and the contact resistance between the material, the electrolyte, and the current collector [52]. The semicircle diameter corresponds to the charge transfer resistance (R_{ct}) of the material [18, 20, 53]. The comparison between the four curves corresponding UV-RGO modified electrodes with different amounts of GR-FMT (0, 40, 80, and 120 mg) shows that the smallest semicircle (corresponding to $R_{ct} = 1.03$ kΩ) is obtained for the 80 mg GR-FMT addition. This condition provides for the fastest interfacial electron transfer and the strongest reduction, which is consistent with XPS and FTIR results [54]. The impedance value of the oxygen-rich GO-modified electrode shows the largest R_{ct} value (2.45 kΩ) corresponding to the slowest interfacial electron transfer.

Cyclic voltammetry (CV) scans have been carried out before EIS measurements to examine the heterogeneous electron transfer (HET) rate of graphene-based materials. Figure 6b compares the CV curves of GO and UV-RGO electrodes with different GR-FMT additions in the same electrolyte solution as EIS. With the addition of GR-FMT, the amperometric response of the redox probe is found to increase while the peak-to-peak separation decreases. It has been widely accepted that the increase of oxygen-containing groups on a material surface tends to lower the HET rate and to increase the peak-to-peak separation ΔE [52, 55, 56]. Clearly, the electron transfer is blocked at GO-modified glassy carbon electrode (GCE) compared to the UV-RGO-modified GCE. The analysis of CV curves of GO with different GR-FMT amounts indicates a highest peak separation of 0.61 V in GO, while this value lowers to 0.57, 0.42, and 0.55 V for a GR-FMT addition of 40, 80, and 120 mg, respectively. The ΔE data give an HET rate order consistent with the EIS results.

Conclusions

In conclusion, a novel facile, time/energy saving, and environmental friendly method for reducing GO is successfully designed. UV-RGO samples are prepared by irradiating with UV-light suspensions in ethanol containing a photoinitiator (GR-FMT) and GO. GR-FMT plays both the roles of the reductant and deoxidant: it allows for a higher reduction efficiency and simpler process compared to TiO$_2$-assisted GO reduction. GO owns the advantage of a facile and large-scale production and great effort has been devoted to making full use of it. This method

represents a new way of transposing the large-scale production of GO to RGO or more generally to preparing graphene.

Acknowledgement

Electronic supplementary material: The online version of this article (doi:10.1007/s10853-016-0721-y) contains supplementary material, which is available to authorized users.

References

[1] Zhu Y, Murali S, Stoller MD, Ganesh KJ, Cai W, Ferreira PJ, Pirkle A, Wallace RM, Cychosz KA, Thommes M, Su D, Stach EA, Ruoff RS (2011) Carbon-based supercapacitors produced by activation of graphene. Science 332(6037):1537–1541

[2] Cao XH, Shi YM, Shi WH, Lu G, Huang X, Yan QY, Zhang QC, Zhang H (2011) Preparation of novel 3D graphene networks for supercapacitor applications. Small 7(22):3163–3168

[3] Brownson DAC, Kampouris DK, Banks CE (2012) Graphene electrochemistry: fundamental concepts through to prominent applications. Chem Soc Rev 41(21):6944–6976

[4] He QY, Wu SX, Gao S, Cao XH, Yin ZY, Li H, Chen P, Zhang H (2011) Transparent, flexible, all-reduced graphene oxide thin film transistors. ACS Nano 5(6):5038–5044

[5] Radich JG, Krenselewski AL, Zhu JD, Kamat PV (2014) Is graphene a stable platform for photocatalysis? mineralization of reduced graphene oxide With UV-irradiated TiO_2 nanoparticles. Chem Mater 26(15):4662–4668

[6] Huang CC, Li C, Shi GQ (2012) Graphene based catalysts. Energy Environ Sci 5(10):8848–8868

[7] Cho SH, Yang HN, Lee DC, Park SH, Kim WJ (2013) Electrochemical properties of Pt/graphene intercalated by carbon black and its application in polymer electrolyte membrane fuel cell. J Power Sources 225(225):200–206

[8] Sudibya HG, He Q, Zhang H, Chen P (2011) Electrical detection of metal ions using field-effect transistors based on micropatterned reduced graphene oxide films. ACS Nano 5(3):1990–1994

[9] Wang M, Fu L, Gan L, Zhang CH, Rümmeli M, Bachmatiuk A, Huang K, Fang Y, Liu ZF (2013) CVD growth of large area smooth-edged graphene nanomesh by nanosphere lithography. Sci Rep 3:1238

[10] Zhang CH, Zhao SL, Jin CH, Koh AL, Zhou Y, Xu WG, Li QC, Xiong QH, Peng HL, Liu ZF (2015) Direct growth of large-area graphene and boron nitride heterostructures by a co-segregation method. Nat Commun 6:6519

[11] Novoselov KS, Geim AK, Morozov SV, Jiang D, Zhang Y, Dubonos SV, Grigorieva IV, Firsov AA (2004) Electric field effect in atomically thin carbon films. Science 306(5696):666–669

[12] Pang SP, Englert JM, Tsao HN, Hernandez Y, Hirsch A, Feng XL, Mullen K (2010) Extrinsic corrugation-assisted mechanical exfoliation of monolayer graphene. Adv Mater 22(47):5374–5377

[13] Jiao LY, Wang XR, Diankov G, Wang HL, Dai HJ (2010) Facile synthesis of high-quality graphene nanoribbons. Nat Nanotechnol 5(5):321–325

[14] Kosynkin DV, Higginbotham AL, Sinitskii A, Lomeda JR, Dimiev A, Price K, Tour JM (2009) Longitudinal unzipping of carbon nanotubes to form graphene nanoribbons. Nature 458(7240):872–876

[15] Berger C, Song Z, Li T, Li X, Ogbazghi AY, Feng R, Dai Z, Marchenkov AN, Conrad EH, First PN, de Heer WA (2004) Ultrathin epitaxial graphite: 2D electron gas properties and a route toward graphene-based nanoelectronics. J Phys Chem B 108(52):19912

[16] Park S, Ruoff RS (2010) Chemical methods for the production of graphenes. Nat Nanotechnol 5(4):217–224

[17] Loh KP, Bao Q, Ang PK, Yang J (2010) The chemistry of graphene. J Mater Chem 20(12):2277–2289

[18] Chua CK, Pumera M (2013) Reduction of graphene oxide with substituted borohydrides. J Mater Chem A 1(5):1892–1898

[19] Gao J, Liu F, Liu YL, Ma N, Wang ZQ, Zhang X (2010) Environment-friendly method to produce Graphene that employs Vitamin C and amino acid. Chem Mater 22(7):2213–2218

[20] Chua CK, Ambrosi A, Pumera M (2012) Graphene oxide reduction by standard industrial reducing agent: thiourea Dioxide. J Mater Chem 22(22):11054–11061

[21] Salas EC, Sun Z, Lüttge A, Tour JM (2010) Reduction of Graphene Oxide via bacterial respiration. ACS Nano 4(8):4852–4856

[22] Guo C, Book-Newell B, Irudayaraj J (2011) Protein-directed reduction of graphene oxide and intracellular imaging. Chem Commun 47(47):12658–12660

[23] Zhou X, Zhang J, Wu H, Yang H, Zhang J, Guo S (2011) Reducing Graphene Oxide via hydroxylamine: a simple and efficient route to Graphene. J Phys Chem C 115(24):11957–11961

[24] Ambrosi A, Chua CK, Bonanni A, Pumera M (2012) Lithium Aluminum hydride as reducing agent for chemically reduced Graphene Oxides. Chem Mater 24(12):2292–2298

[25] Ren PG, Yan DX, Ji X, Chen T, Li ZM (2011) Temperature dependence of graphene oxide reduced by hydrazine hydrate. Nanotechnol 22(5):055705–055712

[26] Akhavan O (2010) The effect of heat treatment on formation of Graphene thin films from Graphene Oxide nanosheets. Carbon 48(2):509–519

[27] Chen W, Yan L, Bangal PR (2010) Preparation of Graphene by the rapid and mild thermal reduction of Graphene Oxide induced by microwaves. Carbon 48(4):1146–1152

[28] Zhou M, Wang YL, Zhai YM, Zhai JF, Ren W, Wang F, Dong SJ (2009) Controlled synthesis of large-area and patterned electrochemically reduced graphene oxide films. Chem Eur J 15(25):6116–6120

[29] Strong V, Dubin S, Elkady MF, Lech A, Wang Y, Weiller BH, Kaner RB (2012) Patterning and electronic tuning of laser scribed graphene for flexible all-carbon devices. ACS Nano 6(2):1395–1403

[30] Trusovas R, Ratautas K, Račiukaitis G, Barkauskas J, Stankevičienė I, Niaura G, Mažeikienė R (2013) Reduction of graphite oxide to graphene with laser irradiation. Carbon 52(1):574–582

[31] ZhangYL Guo L, Xia H, Chen QD, Feng J, Sun HB (2014) Photoreduction of graphene oxides: methods, properties, and applications. Adv Opt Mater 2(1):10–28

[32] Williams G, Seger B, Kamat PV (2008) TiO$_2$-Graphene Nanocomposites. UV-assisted photocatalytic reduction of graphene oxide. ACS Nano 2(7):1487–1491

[33] Akhavan O, Abdolahad M, Esfandiar A, Mohatashamifar M (2010) Photodegradation of graphene oxide sheets by TiO$_2$ nanoparticles after a photocatalytic reduction. J Phys Chem C 114(30):12955–12959

[34] Degirmenci M, Onen A, Yagci Y, Pappas SP (2001) Photoinitiation of cationic polymerization by visible light activated titanocene in the presence of onium salts. Polym Bull 46(6):443–449

[35] Lin SH, Hsiao YN, Hsu KY (2009) Preparation and characterization of Irgacure 784 doped photopolymers for holographic data storage at 532 nm. J Opt A: Pure Appl Opt 11(2):24012–24020

[36] Itakura T, Torigoe K, Esumi K (1995) Preparation and characterization of ultrafine metal particles in ethanol by UV irradiation using a photoinitiator. Langmuir 11(10):4129–4134

[37] Hummers WS, Offeman RE (1958) Preparation of graphitic oxide. J Am Chem Soc 80(6):1339

[38] Giuffrida S, Condorelli GG, Costanzo LL, Fragala IL, Ventimiglia G, Vecchio G (2004) Photochemical mechanism of the formation of nanometer-sized copper by UV irradiation of ethanol bis(2,4-pentanedionato)copper(II) solutions. Chem Mater 16(7):1260–1266

[39] Condorelli GG, Costanzo LL, Fragala IL, Giuffrida S, Ventimiglia G (2003) A single photochemical route for the formation of both copper nanoparticles and patterned nanostructured films. J Mater Chem 13(10):2409–2411

[40] Celiešiūtė R, Trusovas R, Niaura G, Švedas V, Račiukaitis G, Ruželė Ž, Pauliukaite R (2014) Influence of the laser irradiation on the electrochemical and spectroscopic peculiarities of graphene-chitosan composite. Electrochim Acta 132(19):265–276

[41] Ferrari AC, Robertson J (2000) Interpretation of Raman spectra of disordered and amorphous carbon. J Phys Rev B 61(20):14095–14107

[42] Cancado LG, Jorio A, Ferreira EH, Stavale F, Achete CA, Capaz RB, Mountinho MV, Lombardo A, Kulmala TS, Ferrari AC (2011) Quantifying defects in graphene via Raman spectroscopy at different excitation energies. Nano Lett 11(8):3190–3196

[43] Tang H, Gao PB, Bao ZH, Zhou B, Shen J, Mei YF, Wu GM (2015) Conductive resilient graphene aerogel via magnesiothermic reduction of graphene oxide assemblies. Nano Res 8(5):1710–1717

[44] Min SX, Lu GX (2011) Dye-sensitized reduced graphene oxide photocatalysts for highly efficient visible-light-driven water reduction. J Phys Chem C 115(28):13938–13945

[45] Shin HJ, Kim KK, Benayad A, Yoon SM, Park HK, Jung IS, Jin MH, Jeong HK, Kim JM, Choi JY, Lee YH (2009) Efficient reduction of graphite oxide by sodium borohydride and its effect on electrical conductance. Adv Funct Mater 19(12):1987–1992

[46] Zhang YP, Pan CX (2011) TiO$_2$/graphene composite from thermal reaction of graphene oxide and its photocatalytic activity in visible light. J Mater Sci 46(8):2622–2626. doi:10.1007/s10853-010-5116-x

[47] Sabol D, Gleeson MR, Liu S, Sheridan JT (2010) Photoinitiation study of Irgacure 784 in an epoxy resin photopolymer. J Appl Phys 107(5):053113–053118

[48] Howe RF, Graetzel M (1985) EPR observation of trapped electrons in colloidal TiO$_2$. J Phys Chem 89(21):4495–4499

[49] Ligon SC, Husár B, Wutzel H, Holman R, Liska R (2013) Strategies to reduce oxygen inhibition in photoinduced polymerization. Chem Rev 114(1):557–589

[50] Becerril HA, Mao J, Liu Z, Stoltenberg RM, Bao Z, Chen Y (2008) Evaluation of solution-processed reduced graphene oxide films as transparent conductors. ACS Nano 2(3):463–470

[51] Mazánek V, Jankovský O, Luxa J, Sedmidubský D, Janoušek Z, Šembera F, Mikulicsc M, Sofer Z (2015) Tuning of

fluorine content in graphene: towards large-scale production of stoichiometric fluorographene. Nanoscale 7(32):13646–13655

[52] Dubal DP, Holze R (2013) All-solid-state flexible thin film supercapacitor based on Mn_3O_4 stacked nanosheets with gel electrolyte. Energy 51(2):407–412

[53] Ambrosi A, Bonanni A, Sofer Z, Cross JS, Pumera M (2011) Electrochemistry at chemically modified graphenes. Chem Eur J 17(38):10763–10770

[54] Cao XR, Tian GH, Chen YJ, Zhou J, Zhou W, Tian CG, Fu HG (2014) Hierarchical composites of TiO_2 nanowire arrays on reduced graphene oxide nanosheets with enhanced photocatalytic hydrogen evolution performance. J Mater Chem A 2(12):4366–4374

[55] Nicholson RS (1965) Theory and application of cyclic voltammetry for measurement of electrode reaction kinetics. Anal Chem 37(11):1351–1355

[56] Konopka SJ, McDuffie B (1970) Diffusion coefficients of ferri- and ferrocyanide ions in aqueous media, using twin-electrode thin-layer electrochemistry. Anal Chem 42(14):1741–1746

[57] Wang GX, Yang J, Park JS, Gou XL, Wang B, Liu H, Yao J (2008) Facile synthesis and characterization of graphene nanosheets. J Phys Chem C 112(22):8192–8195

[58] Abdelsayed V, Moussa S, Hassan HM, Aluri HS, Collinson MM, El-Shall MS (2010) Photothermal deoxygenation of graphene oxide with laser excitation in solution and graphene-aided increase in water temperature. J Phys Chem Lett 1(19):2804–2809

[59] Zhou Y, Bao QL, Varghese B, Tang LAL, Tan CK, Sow CH, Loh KP (2010) Microstructuring of graphene oxide nanosheets using direct laser writing. Adv Mater 22(1):67–71

[60] Prezioso S, Perrozzi F, Donarelli M, Bisti F, Santucci S, Palladino L, Nardone M, Treossi E, Palermo V, Ottaviano L (2012) Large area extreme-UV lithography of graphene oxide via spatially resolved photoreduction. Langmuir 28(12):5489–5495